DOI: 10.13009/EUCASS2022-4753
9TH EUROPEAN CONFERENCE FOR AERONAUTICS AND SPACE SCIENCES (EUCASS)

A near-wall control approach to suppress the log-law energy containing structures to obtain frictional drag reduction at relatively high Reynolds numbers

Atilla Altıntaş[1]†, *Lars Davidson*[1] *and Shia-Hui Peng*[1–2]
[1]*Division of Fluid Dynamics, Department of Mechanics and Maritime Sciences*
Chalmers University of Technology, 412 96 Gothenburg, Sweden
[2]*Swedish Defence Research Agency, FOI, SE-164 90 Stockholm, Sweden*
†altintas@chalmers.se
†Corresponding author

Abstract

The energy consumption of an aircraft in flight is mainly due to the aerodynamic drag force. The viscous drag, which directly related to the friction drag, is responsible for almost half of the total drag. At high Reynolds numbers, the energy containing structures in the log-law region are highly effective in enhancing the near-wall turbulence. In this study a near-wall control approach is applied and explored to a turbulent channel flow which suppresses the positive wall-normal fluctuations to manipulate the interplay between the log-law and near-wall turbulent structures. The results show significant drag reduction which is related to the absence of the large-scale (LS) motions in the log-law region.

1. Introduction

The aerodynamic drag force is the main reason of the energy consumption that opposes an aircraft's motion through the air. Almost 50% of total drag is due to the viscous drag, which is directly related to the friction drag of the aircraft caused by the interaction of the turbulent boundary layer flow with the aircraft surface. Studies on the aircraft and turbulent boundary layer interactions, together with developments of advanced flow control technologies, can effectively reduce more than 40% of the viscous drag, which is equivalent to about 20% of the total drag and has, therefore, major implications to the energy consumption of commercial aircraft. Saving 1% of fuel on a Boeing 737 − 800 would result in a 100 metric tons yearly fuel reduction. It would also decrease the emission of pollutants by 318.7 tons of CO_2, 123.9 tons of H_2O, 2.122 tons of NO_x , 98 kg of SO_2 and 56 kg of CO. Hence, even a small drag reduction gives significant benefits [1]. Many studies have addressed the existence of LS motions that are very important for wall turbulence at high Reynolds numbers [4, 17]. The streamwise lengths of the large eddies can be in an order of 10-20 boundary-layer thicknesses in the logarithmic region of wall-bounded flows [15]. These large eddies involve mostly streamwise velocity fluctuations and contain most of the streamwise kinetic energy. Many subsequent studies have reported that log-law LS motions strongly influence near-wall turbulent structures [2, 4, 10, 12, 17, 18, 22]. Therefore, to control the log-law large-scale structures is important to obtain frictional drag reduction at high Reynolds numbers. However, the general approach to control those log-law structures is to apply a flow control method on those relatively high wall-normal locations. This is not a feasible method when it comes to real-world applications.

In this study, we suppressed positive wall-normal velocity near the wall, at $y^+ < 20$. By doing so we aimed to suppress the formation or interaction of organized flow structures in the log-law region. This study is performed for a frictional Reynolds number of $Re_\tau = 550$, it is also supported with a higher Reynolds number, $Re_\tau = 800$. A high amount of drag reduction is observed for the controlled case (43% and 45% for $Re_\tau = 550$ and $Re_\tau = 800$, respectively) that is related to the absence of the streak formations in the log-law region. The streak formations are compared for the controlled and uncontrolled cases at the inner and outer kinetic energy peak locations. We observed that the streak formations are reduced/suppressed in the log-law region. This conclusion is supported by the two-point velocity correlations and streamwise velocity contour plots. We quantify the difference in the effect of the log-law influence on the wall-turbulence for the controlled and uncontrolled applied cases by amplitude modulation analysis. The 'modulation effect' is one of two commonly accepted effects of the outer LS structures on near-wall turbulent fluctuations. Amplitude modulation analysis is a method to understand how LS motions amplify or attenuate the turbulent structures near the wall. We compare the amplitude modulation for the uncontrolled and the controlled cases

DOI: 10.13009/EUCASS2022-4753

for both $Re_\tau = 550$ and $Re_\tau = 800$, and we obtain a much lower correlation between the LS and near-wall structures for the controlled cases compared to uncontrolled cases.

The paper is organized as follows. First, a brief description of the numerical method is presented, followed by the presentation and discussion of the results. Finally concluding remarks are given in the last section.

2. Direct Numerical Simulations

A flow solver with an implicit, two-step time-advancement finite volume methods is used [8]. Central differencing is used in space and the Crank-Nicolson scheme is used in the time domain. When the Navier-Stokes equation is discretized for u_i it can be written as,

$$u_i^{n+1} = u_i^n + \Delta t H\left(u_i^n, u_i^{n+1}\right) - \frac{1}{\rho}\alpha\Delta t \frac{\partial p^{n+1}}{i} - \frac{1}{\rho}(1-\alpha)\Delta t \frac{\partial p^n}{i} \tag{1}$$

where $H\left(u_i^n, u_i^{n+1}\right)$ includes convection, the viscous and the source terms, and $\alpha = 0.5$ (Crank-Nicolson). Equation 1 is solved which gives u_i^{n+1} which does not satisfy continuity. An intermediate velocity field is computed by subtracting the implicit part of the pressure gradient, i.e.

$$u_i^* = u_i^{n+1} + \frac{1}{\rho}\alpha\Delta t \frac{\partial p^{n+1}}{i}. \tag{2}$$

Taking the divergence of Eq. 2 requiring that continuity (for the face velocities which are obtained by linear interpolation) should be satisfied on level $n+1$, i.e. $\partial u_{i,f}^{n+1}/_i = 0$, we obtain

$$\frac{\partial^2 p^{n+1}}{ii} = \frac{\rho}{\Delta t \alpha} \frac{\partial u_{i,f}^*}{i}. \tag{3}$$

The numerical procedure at each time step can be summarized as follows [20].

1. Solve the discretized filtered Navier-Stokes equation for u, v and w.
2. Create an intermediate velocity field u_i^* from Eq. 2.
3. The Poisson equation (Eq. 3) is solved with an efficient multigrid method [9].
4. Compute the face velocities (which satisfy continuity) from the pressure and the intermediate velocity as

$$u_{i,f}^{n+1} = u_{i,f}^* - \frac{1}{\rho}\alpha\Delta t \left(\frac{\partial p^{n+1}}{i}\right)_f. \tag{4}$$

5. Step 1 to 4 is performed till convergence (normally two or three iterations) is reached. The convergence for the velocities is 10^{-7} and 10^{-5} for pressure. The residuals are computed using $L1$ norm and they are scaled with the integrated streamwise volume flux (continuity equation) and momentum flux (momentum equations).
6. Next time step.

Note that although no explicit dissipation is added to prevent odd-even decoupling, an implicit dissipation is present. The intermediate velocity field is computed at the *cell centres* (see Eq. 2) subtracting a pressure gradient. When, after having solved the pressure Poisson equation, the face velocity field is computed, the pressure gradient at the *faces* (see Eq. 4) is added. This is very similar to the Rhie-Chow dissipation [21].

A constant volumetric driving force is used in the streamwise momentum equation by which the frictional Reynolds number, $Re_\tau = 550$ and $Re_\tau = 800$ is prescribed. Periodic boundary conditions are used in the streamwise and spanwise directions, while the usual no-slip boundary conditions are enforced at the walls. The domain size is $2\pi\delta \times 2\delta \times \pi\delta$ for both cases, with grid sizes $258 \times 194 \times 258$ and $386 \times 258 \times 386$, respectively for the $Re_\tau = 550$ and $Re_\tau = 800$ cases, in the streamwise, wall-normal and spanwise directions. The grid resolution is $\Delta x^+ \approx 13, \Delta z^+ \approx 6$, for both cases and a stretching of 1.03 is used in the wall-normal direction.

The nondimensional time step was kept smaller than $\Delta t^+ = \Delta t u_\tau^2/\nu = 0.6$. The variables u, v, w represent the streamwise, wall-normal and spanwise velocities, respectively. The results are, unless otherwise stated, averaged in all homogeneous directions (i.e. x_1, x_3 and t); the average is denoted by an overbar $(\bar{\cdot})$.

DOI: 10.13009/EUCASS2022-4753

2.1 First Order Statistics

Figures 1(a), 1(b) and Figs. 2(a), 2(b) present the mean velocity and resolved turbulent fluctuations for $Re_\tau = 550$ and $Re_\tau = 800$; they are compared with DNS data of Jimenez et al. [13] and Tanahashi et al. [24], respectively and as can be seen, the agreement is good.

Drag histories, i.e. wall shear stresses, are presented in Figs. 3(a) and 3(b) for the uncontrolled cases for the $Re_\tau = 550$ and $Re_\tau = 800$, respectively, and they oscillates around 1. The drag histories are given separately for the north (upper) and south (lower) wall, since the control is applied to the south wall (see section 3).

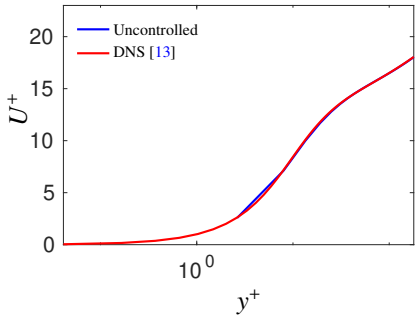

(a) Mean velocity, U^+ profile, uncontrolled.

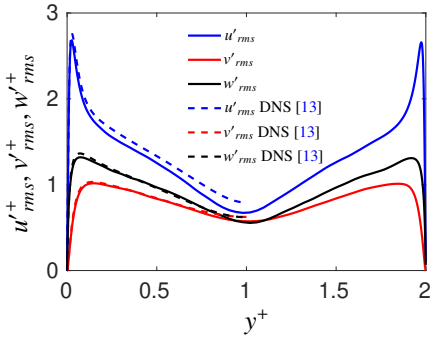

(b) Velocity fluctuations.

Figure 1: Mean velocity and fluctuations. $Re_\tau = 550$.

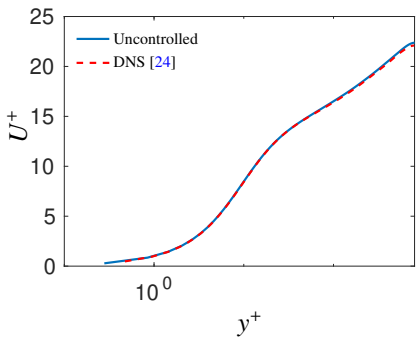

(a) Mean velocity, U^+ profile, uncontrolled.

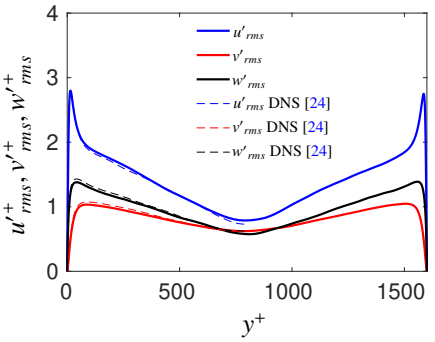

(b) Velocity fluctuations.

Figure 2: Mean velocity and fluctuations. $Re_\tau = 800$.

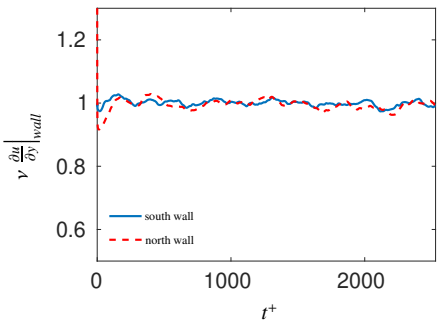

(a) $Re_\tau = 550$.

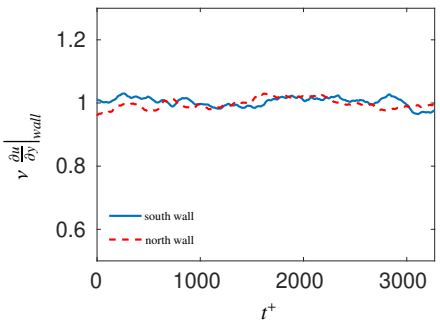

(b) $Re_\tau = 800$.

Figure 3: Drag history for the no-force cases.

DOI: 10.13009/EUCASS2022-4753

3. Results

The positive wall velocities are suppressed near the wall ($y+ < 20$) in the controlled case, i.e when the wall-normal velocity, v, is positive a source term, $-\rho v/\Delta t$, is added at $y^+ < 20$. As a result significant drag reduction is observed for both two cases, which is 43% for $Re_\tau = 550$ and 40% for $Re_\tau = 800$ (Figs 4(a) and 4(b)).

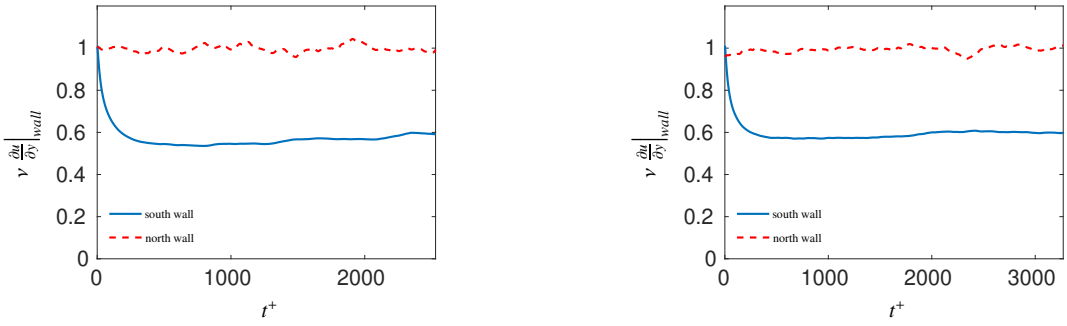

(a) $Re_\tau = 550$. (b) $Re_\tau = 800$.

Figure 4: Drag history for the control applied cases.

The regeneration cycle of low-speed streaks and streamwise vortices, namely, the "streak cycle" is investigated by Hamilton et al. [11] and Jiménez and Pinelli [14]. In their study they showed that the cycle is governed by the streak instability which generates tilted streamwise vortices. The streamwise vortices in turn assemble low-speed fluid and generate low speed streaks. These streaks undergo wavy motions and lead to streak instability. The control applied in this study aims to diminish the streak formation in the log-law region by suppressing the well known bursts mechanism. It is known that the bursting process could be described by three stages, namely, lifting of a low-speed streak from the wall, oscillation of the gradually migrated low-speed streaks away from the wall and finally 'break up' of the streaks [16]. The break up, the last stage of the bursting process, is also known as the beginning of the 'cascade' processes that creates smaller fluctuations. In the second stage of bursting, also known as oscillatory growth motion, the dominant mode is streamwise vortices, in which vortex size grow and their strength increase [16]. The bursting process is responsible for 70% of the turbulence production near the wall [16].

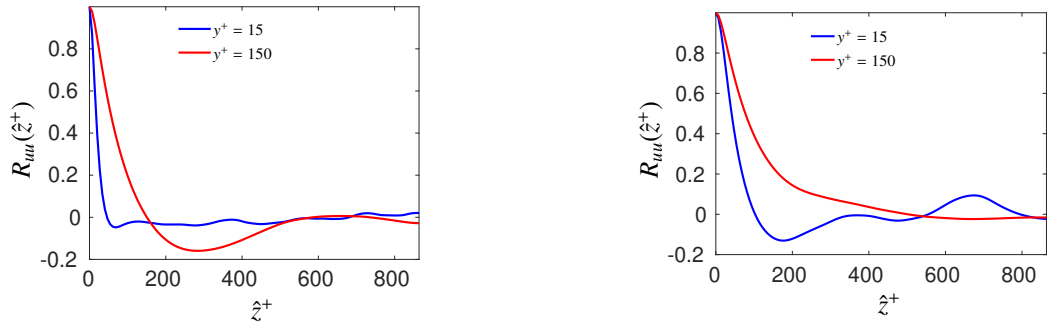

(a) Uncontrolled. (b) Controlled.

Figure 5: Streamwise two-point velocity correlations. $Re_\tau = 550$.

Two-point correlations are applied to analyze the change of the streaky structures both near the wall and at the log-law region. Streamwise velocity two-point correlation, $R_{uu}(\hat{z}^+)$, carries information on the mean spacing between the high and low-speed streaks. The location of the minimum of the $R_{uu}(\hat{z}^+)$ provides an estimate of the mean separation between the high and the low speed fluid; the mean spacing between the streaks of high and low speed fluid is roughly twice of that separation [7]. In Figs. 5 and 6, the streamwise velocity two-point correlations, $R_{uu}(\hat{z}^+)$, are shown for $Re_\tau = 550$ and $Re_\tau = 800$, respectively.

For $Re_\tau = 550$, for the uncontrolled case, the minimum value for the correlation is observed approximately at $\hat{z}^+ = 54$ for $y^+ = 15$, and at $\hat{z}^+ = 300$ for $y^+ = 150$ (Fig. 5(a)). The locations $y^+ = 15$ and $y^+ = 150$ are the locations of the peaks of high turbulent kinetic energy for the near-wall and log-law region (see Figs. 10 and 11). In controlled case the minimum of the $R_{uu}(\hat{z}^+)$ for $y^+ = 15$ shifts to approximately $\hat{z}^+ = 180$, hence, the streaky structures seem to be modified to larger forms in the spanwise direction near the wall. The controlled case exhibit a faint minimum at

DOI: 10.13009/EUCASS2022-4753

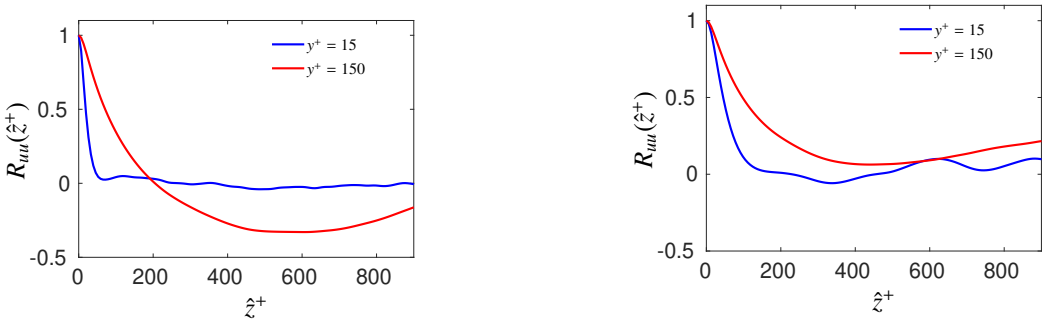

(a) Uncontrolled. (b) Conrolled.

Figure 6: Streamwise two-point velocity correlations. $Re_\tau = 800$.

$y^+ = 150$ at a larger distance of about $\hat{z}^+ = 600$ which indicates the absence of streaky structures or more stable or weak streaky structures in the log-law region [7] (a similar modification is observed for $Re_\tau = 800$ see Fig. 6(a) and Fig. 6(b)).

The enlargement of the streaks near the wall can also be seen in Fig. 7(a) compared to Fig. 7(b) which presents the streamwise velocity contours at $y^+ = 15$ for the $Re_\tau = 550$. For $y^+ = 150$ the low-speed streaks seem disappear (Fig. 8(a) compared to Fig. 8(b)). The disappearence of the streaks at $y^+ = 150$ supports the idea that the cascade process is manipulated by the disapearence of the low-speed streaks that generate the energy dissipated to the lower locations in the wall-normal direction. For having further insight the turbulent and mean dissipation as well as the turbulence production are investigated below.

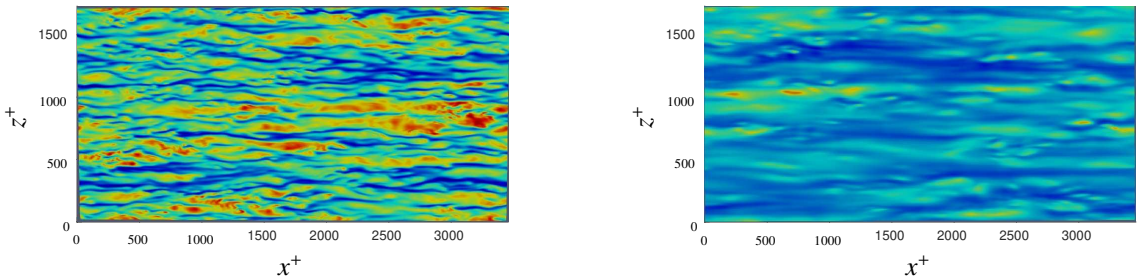

(a) Uncontrolled case. (b) Controlled case.

Figure 7: Streamwise velocity (u) contours for the controlled and uncontrolled cases, $y^+ = 15$. Blue indicates low speed streaks and yellow-red high speed streaks. $Re_\tau = 550$.

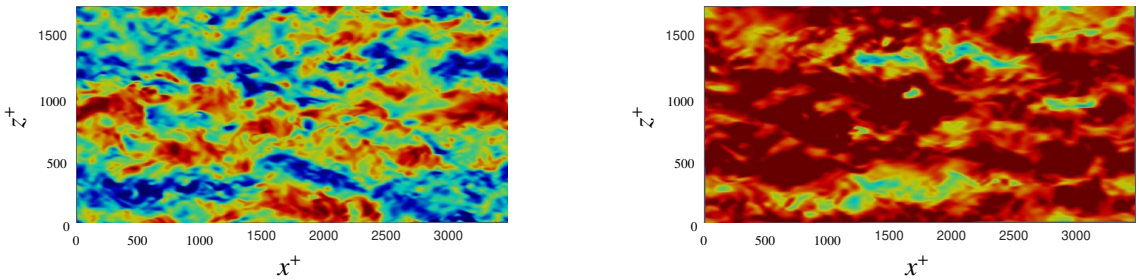

(a) Uncontrolled case. (b) Controlled case.

Figure 8: Streamwise velocity (u) contours for the controlled and uncontrolled cases, $y^+ = 150$. Blue indicates low speed streaks and yellow-red high speed streaks. $Re_\tau = 550$.

The local (pointwise) entropy generation rate per unit volume, S''', is a tool to investigate the energy loses. Viscous dissipation of the mean-flow kinetic energy, ε_{mean}, and dissipation of turbulent kinetic energy into thermal

DOI: 10.13009/EUCASS2022-4753

energy ("indirect" or turbulent dissipation), ε, together gives the pointwise entropy generation rate, S''', are considered. For turbulent flow, the time-mean value of dissipation at a point may be expanded to

$$\mu\ \phi + \rho\ \varepsilon$$

where the former represents viscous dissipation of mean-flow kinetic energy (called "direct dissipation") and the latter represents dissipation of turbulent kinetic energy into thermal energy ("indirect" or turbulent dissipation) [6, 23],

$$\rho\ \varepsilon = 2\ \mu \left[\overline{(\frac{\partial u'}{\partial x})^2} + \overline{(\frac{\partial v'}{\partial y})^2} + \overline{(\frac{\partial w'}{\partial z})^2} \right] + \mu \left[\overline{(\frac{\partial u}{\partial y} + \frac{\partial v'}{\partial x})^2} + \overline{(\frac{\partial v'}{\partial z} + \frac{\partial w'}{\partial y})^2} + \overline{(\frac{\partial w'}{\partial x} + \frac{\partial u'}{\partial z})^2} \right] \tag{5}$$

In wall units, the pointwise entropy generation rate for a fully-developed turbulent flow between infinitely-wide parallel plates can be written as [19],

$$(S'''(y^+))^+ = (\frac{\partial U^+}{\partial y^+})^2 + \varepsilon^+ \tag{6}$$

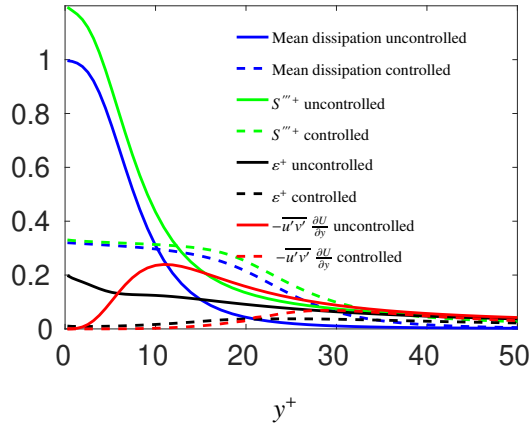

Figure 9: Mean Dissipation, $\nu(\partial U^+/\partial y^+)^2$, turbulent dissipation, ε^+, and volumetric entropy generation rate, $(S'''(y^+))^+$, turbulence production, $-\overline{u'v'}\ \frac{\partial U}{\partial y}$, for uncontrolled and controlled cases for $Re_\tau = 550$.

Figure 9 shows a significant reduction for both the mean and turbulent dissipation for the controlled case compared to the uncontrolled case. In controlled case the turbulent dissipation is so low that the volumetric entropy generation, $(S'''(y^+))^+$, almost matching with the mean dissipation. A significant reduction is observed for the turbulence production for the controlled case compared to the uncontrolled case.

The absence of the streak formations in the log-law region is the main source of drag reduction in the present study. Amplitude modulation refers to the modulation of a high-frequency signal (carrier signal) with a low-frequency component (modulating signal). The modulation effect for the turbulent fluid flow refers to the amplification or attenuation of near-wall small-scale (SS) structures by the LS motions in the log-law region [4]. Thus, investigating and comparing the modulation effect for the uncontrolled and controlled cases will shed light of contribution of the absence of the log-law streaks on the drag reduction obtained. The degree of correlation is quantified by the correlation coefficient

$$R = \frac{\overline{u_L^+\ E_L(u_S^+)}}{\sqrt{u_L^{+2}}\ \sqrt{E_L(u_S^+)^2}},$$

where E denotes the envelope of the signal.The subscripts, 'i','o','S','L', represent the 'inner','outer','small-scale' and 'large-scale'. For instance $u^+_{i,S}$ and $u^+_{i,L}$ represent the small and large scales for the inner peak location ($y^+ = 15$), respectively. For the outer peak location, $u^+_{o,S}$ and $u^+_{o,L}$ give small and large-scales, respectively.

To investigate the modulation effect in the velocity signal, the latter must be decomposed into large and small scales. To do this, one can refer to (i) proper mode decomposition and (ii) filtering by defining the cutoff wavelength that separates the large and small scales. Mathis et al.[17] proposed what is now a widely used method for analyzing amplitude modulation, in which filtering is used to decompose the signal. In this study Hilbert transform together with empirical mode decomposition is applied to decompose velocity signal into large and small scale components [4].

To analyse the change in the energy containing structures in the near-wall and log-law region the location of these structures need to be defined. To obtain the high energy locations we applied to pre-multiplied energy spectra

DOI: 10.13009/EUCASS2022-4753

maps for both the $Re_\tau = 550$ and $Re_\tau = 800$ (Figs. 10 and 11). The energy peak which is located in the near-wall region is called the 'inner peak', accepted as the energetic signature of the near-wall cycle of turbulence production [5, 17]. In Figs. 10(a) and 11(a), this inner peak is located at around $y^+ = 15$ and $\lambda_z^+ = 100$ for both two Reynolds number cases. The so called 'outer peak' is located in the logaritmic region and accepted as the energetic signature of the large-scale organization of the velocity field (superstructures). In Fig. 10(a), for the $Re_\tau = 550$ this outer energy peak is located around $y^+ = 150$ and $\lambda_z^+ = 500$. For the $Re_\tau = 800$ the log-law energy peak is located at $y^+ = 150$ same as $Re_\tau = 550$, while the $\lambda_z^+ = 800$. Figures 10(b) and 11(b) are the energy spectra maps for the controlled cases. For both Reynolds numbers the controlled case exhibits a reduction on the energy level for the log-law. The high energy region in the log-law seems to be weakened and connected with the near-wall energy region compared to Fig. 10(a) with Fig. 10(b), and Fig. 11(a) with Fig. 11(a).

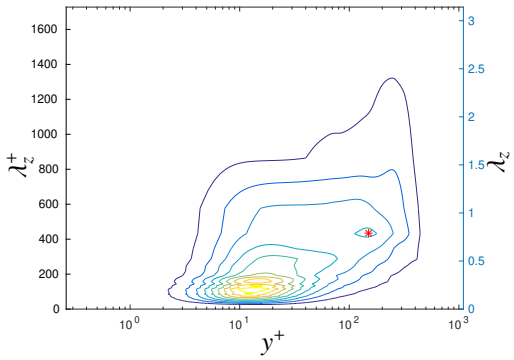

(a) Uncontrolled. *: peak in the outer region.

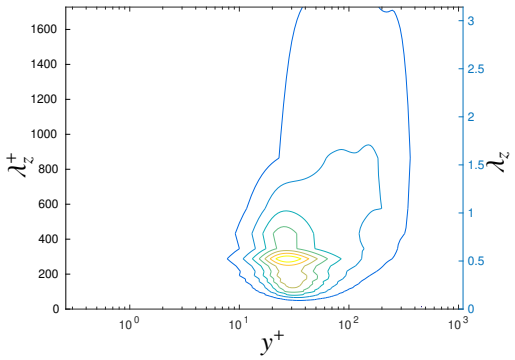

(b) Controlled

Figure 10: Contours of pre-multiplied energy spectra, $k_z\phi_{uu}(k_z)/u_\tau$, for streamwise velocity fluctuations. $Re_\tau = 800$.

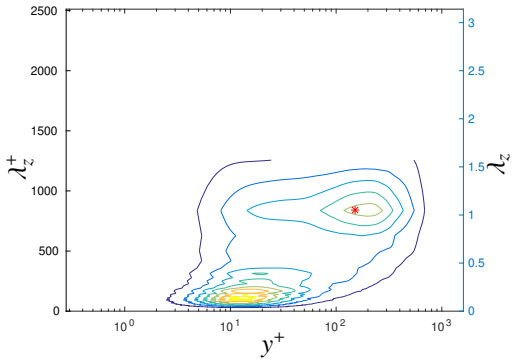

(a) Uncontrolled. *: peak in the outer region.

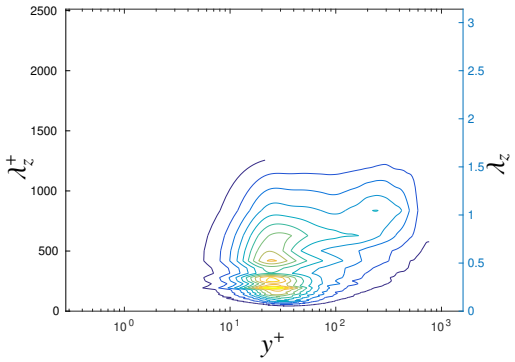

(b) Controlled

Figure 11: Contours of pre-multiplied energy spectra, $k_z\phi_{uu}(k_z)/u_\tau$, for streamwise velocity fluctuations. $Re_\tau = 800$.

For $Re_\tau = 550$, for the uncontrolled case the modulation effect analysis gives a correlation coefficient of $R = 0.2230$, while the controlled case gives, $R = 0.0965$ (Figs. 12(a) and Figs. 12(b)). For $Re_\tau = 800$, for the uncontrolled case the correlation coefficient is $R = 0.2230$, for the controlled case it reads, $R = 0.0965$ (Figs. 13(a) and Figs. 13(b)).

DOI: 10.13009/EUCASS2022-4753

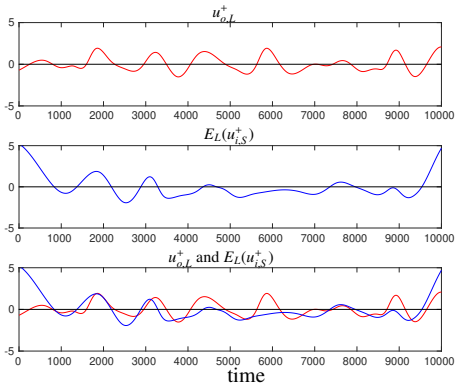

(a) Two-point analysis [4], uncontrolled case, Re_τ = 550.

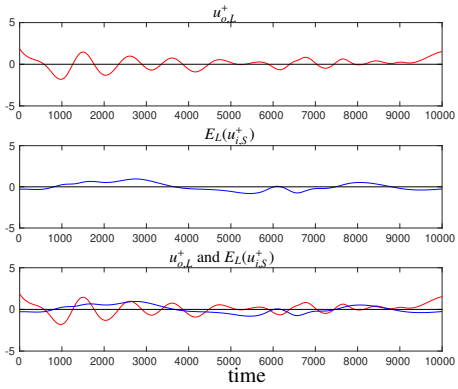

(b) Two-point analysis [4], controlled case, Re_τ = 550.

Figure 12: Correlation for the outer energy peak large-scale structures, $u^+_{o,L}$ and inner small-scale structures, $E_L(u^+_{i,S})$. Re_τ = 550.

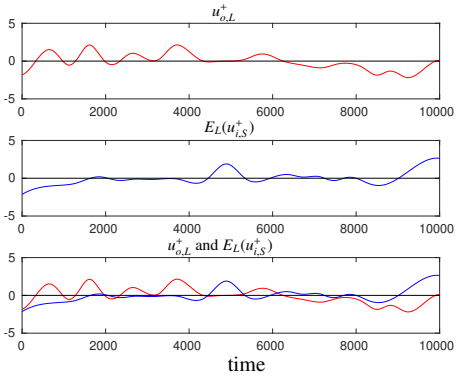

(a) Two-point analysis [4], uncontrolled case, Re_τ = 800.

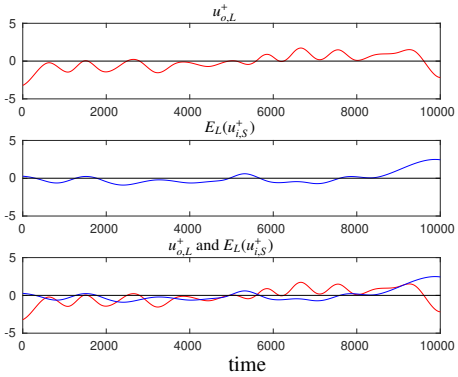

(b) Two-point analysis [4], controlled case, Re_τ = 800.

Figure 13: Correlation for the outer energy peak large-scale structures, $u^+_{o,L}$ and inner small-scale structures, $E_L(u^+_{i,S})$. Re_τ = 800.

4. Conclusion

The effect of the large-scale outer structures on the near-wall turbulence has been addressed by many researchers [2–4, 17]. For increasing Reynolds number, the log-law structures has higher impact on the near-wall turbulence. Therefore to obtain a significant drug reduction at higher Reynolds numbers it is crucial to dampen the aforementioned outer high energy structures. However, in practice, controlling these higher wall-normal locations are very challenging. In this study it has been shown that by suppressing the positive wall-normal velocity near the wall the log-law energy structures can be altered.

The importance of this study is arising from the control of the log-law structures by manipulating the flow in the near-wall area. A suppression of positive wall-normal velocity is applied at $y^+ < 20$. Two Reynolds numbers are used, Re_τ = 550 and Re_τ = 800, the control method is applied to the bottom wall, and 43% and 40% drag reductions are observed, respectively. As a result a significant amount of reduction is observed on the existence of the streaks in the log-law region in the controlled cases compared to the uncontrolled cases.

To study the modulation effect Hilbert-Transfrom and EMD is applied to a temporal data captured over near-wall and log-law energy peak areas. To obtain the location of the energy peak areas pre-multiplied energy spectra maps are plotted for both Reynolds numbers. Amplitude modulation analysis is performed by using EMD (by applying Hilbert-Huang Transform) to investigate the correlation of the LS with SS near-wall structures. In the controlled cases a lower correlation is observed compared to the uncontrolled cases, R = 0.2230, R = 0.0965 and R = 0.106 , R = 0.041 for the uncontrolled and controlled cases for the Re_τ = 550 and Re_τ = 800, respectively.

DOI: 10.13009/EUCASS2022-4753

References

[1] *Guidance Material and Best Practices for Fuel and Environmental Management*. International Air Transport Association, Montreal-Geneva, December, 2004.

[2] L. Agostini and M. Leschziner. Predicting the response of small-scale near-wall turbulence to large-scale outer motions. *Phys. Fluids*, 28:075107–23, 2016.

[3] L Agostini and MA Leschziner. On the influence of outer large-scale structures on near-wall turbulence in channel flow. *Physics of Fluids*, 26(7):075107, 2014.

[4] A. Altıntaş, L. Davidson, and S-H. Peng. A new approximation to modulation-effect analysis based on empirical mode decomposition. *Physics of Fluids*, 31(2):025117, 2019.

[5] M. Bernardini and S. Pirozzoli. Inner/outer layer interactions in turbulent boundary layers: A refined measure for the large-scale amplitude modulation mechanism. *Phys. Fluids*, 23(6):061701–4, 2011.

[6] Tuncer Cebeci and Peter Bradshaw. *Physical and computational aspects of convective heat transfer*. Springer Science & Business Media, 2012.

[7] Haecheon Choi, Parviz Moin, and John Kim. Active turbulence control for drag reduction in wall-bounded flows. *Journal of Fluid Mechanics*, 262:75–110, 1994.

[8] L. Davidson and Peng S-H. Hybrid LES-RANS: A one-equation SGS model combined with a $k - w$ model for predicting recirculating flows. *Int. J. Numer. Fluids*, 43(9):1003–1018, 2003.

[9] P. Emvin and L. Davidson. Development and implementation of a fast large eddy simulations method. Technical report, Dept. of Thermo and Fluid Dynamics, Chalmers University of Technology, Gothenburg, 1997.

[10] B Ganapathisubramani, N Hutchins, JP Monty, D Chung, and I Marusic. Amplitude and frequency modulation in wall turbulence. *Journal of Fluid Mechanics*, 712:61–91, 2012.

[11] J. M. Hamilton, J. Kim, and F. Waleffe. Regeneration mechanism of near-wall turbulence structures. *J. Fluid Mech.*, 287:317–348, 1995.

[12] N Hutchins and Ivan Marusic. Evidence of very long meandering features in the logarithmic region of turbulent boundary layers. *Journal of Fluid Mechanics*, 579:1–28, 2007.

[13] J. Jimenez, S. Hoyas, M. P. Simens, and Y. Mizuno. Turbulent boundary layers and channels at moderate Reynolds numbers. *J. Fluid Mech.*, 657:355–360, 2010.

[14] J. Jiménez and A. Pinelli. The autonomous cycle of near-wall turbulence. *J. Fluid Mech.*, 389:335–359, 1999.

[15] Javier Jiménez, Juan C. Del Alamo, and Oscar Flores. The large-scale dynamics of near-wall turbulence. *Journal of Fluid Mechanics*, 505:179, 2004.

[16] H. T. Kim, S. J. Kline, and W. C. Reynolds. The production of turbulence near a smooth wall in a turbulent boundary layer. *Journal of Fluid Mechanics*, 50(1):133â160, 1971.

[17] R. Mathis, N. Hutchins, and I. Marusic. Large-scale amplitude modulation of the small-scale structures in turbulent boundary layers. *J. Fluid Mech.*, 628:311–337, 2009.

[18] Romain Mathis, Ivan Marusic, Nicholas Hutchins, and KR Sreenivasan. The relationship between the velocity skewness and the amplitude modulation of the small scale by the large scale in turbulent boundary layers. *Physics of Fluids*, 23(12):121702, 2011.

[19] Donald M McEligot, Edmond J Walsh, Eckart Laurien, and Philippe R Spalart. Entropy generation in the viscous parts of turbulent boundary layers. *Journal of Fluids Engineering*, 130(6), 2008.

[20] H. Nilsson. A parallel multiblock extension to the CALC-BFC code using pvm. Technical Report 9711, Dept. of Thermo and Fluid Dynamics, Chalmers University of Technology, Gothenburg, 1984.

[21] CM Rhie and W Li Chow. Numerical study of the turbulent flow past an airfoil with trailing edge separation. *AIAA journal*, 21(11):1525–1532, 1983.

DOI: 10.13009/EUCASS2022-4753

[22] Philipp Schlatter and Ramis Örlü. Quantifying the interaction between large and small scales in wall-bounded turbulent flows: a note of caution. *Physics of fluids*, 22(5):051704, 2010.

[23] Hermann Schlichting and Klaus Gersten. *Boundary layer theory*. Springer, 2015.

[24] M Tanahashi, S-J Kang, T Miyamoto, S Shiokawa, and T Miyauchi. Scaling law of fine scale eddies in turbulent channel flows up to reτ= 800. *International journal of heat and fluid flow*, 25(3):331–340, 2004.